Expanded View Figures

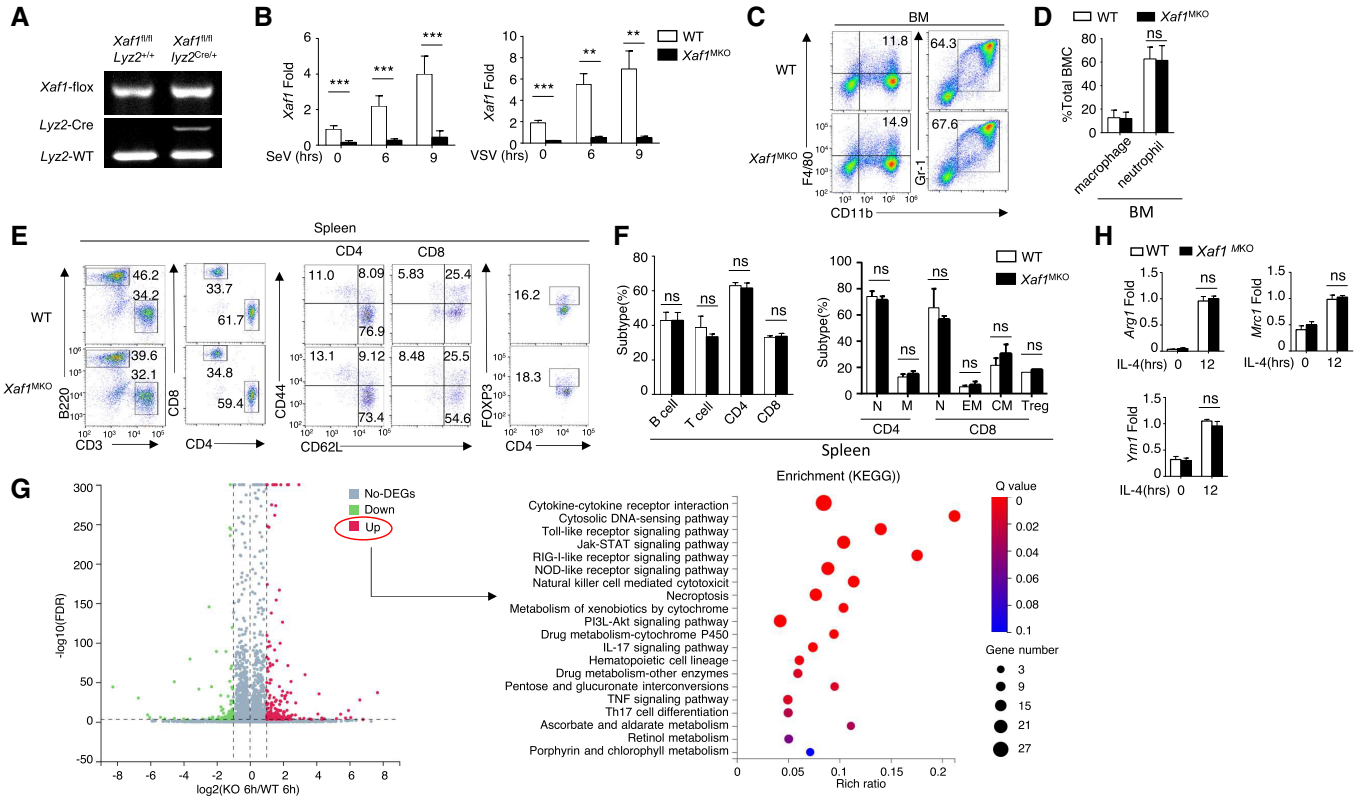

Figure EV1. XAF1 deficiency in myeloid cells had no effect on the development of peripheral immune cells.

A Genotyping PCR of WT ($XAF1^{fl/fl}Lyz2^{+/+}$) and myeloid-conditional XAF1-KO ($XAF1^{MKO}$, $XAF1^{fl/fl}Lyz2^{+/Cre}$) mice.

B qRT–PCR analysis showing clear ablation of XAF1 in the BMDMs of $XAF1^{MKO}$ mice.

C, D Flow cytometry analysis of macrophages ($CD11b^{+}F4/80^{+}$) and neutrophils ($CD11b^{+}Ly6G^{+}$) in bone marrow (BM) from 6- to 8-week-old WT and $XAF1^{MKO}$ mice ($n = 3$).

E, F Flow cytometry analysis of the frequencies of distinct immune cells in the spleen (left), naïve and memory T cells (middle), and Treg cells (right) from WT or $XAF1^{MKO}$ mice ($n = 3$).

G Volcano plot illustrating the upregulated and downregulated DEGs in XAF1-deficient BMDMs compared with WT littermates after 6 h of LPS stimulation. The KEGG analysis showed that the upregulated DEGs were enriched in biological processes.

H qRT–PCR analysis of ARG1, MRC1, and YM1 in IL-4-treated M2 macrophages in WT and XAF1-deficient BMDMs.

Data information: All data are representative of at least three biologically independent experiments. Data from the qPCR assay are presented as the fold change relative to the *Actin* mRNA level. Data are represented as the means ± SDs. The significance of differences was determined by a *t*-test. ns, not significant.

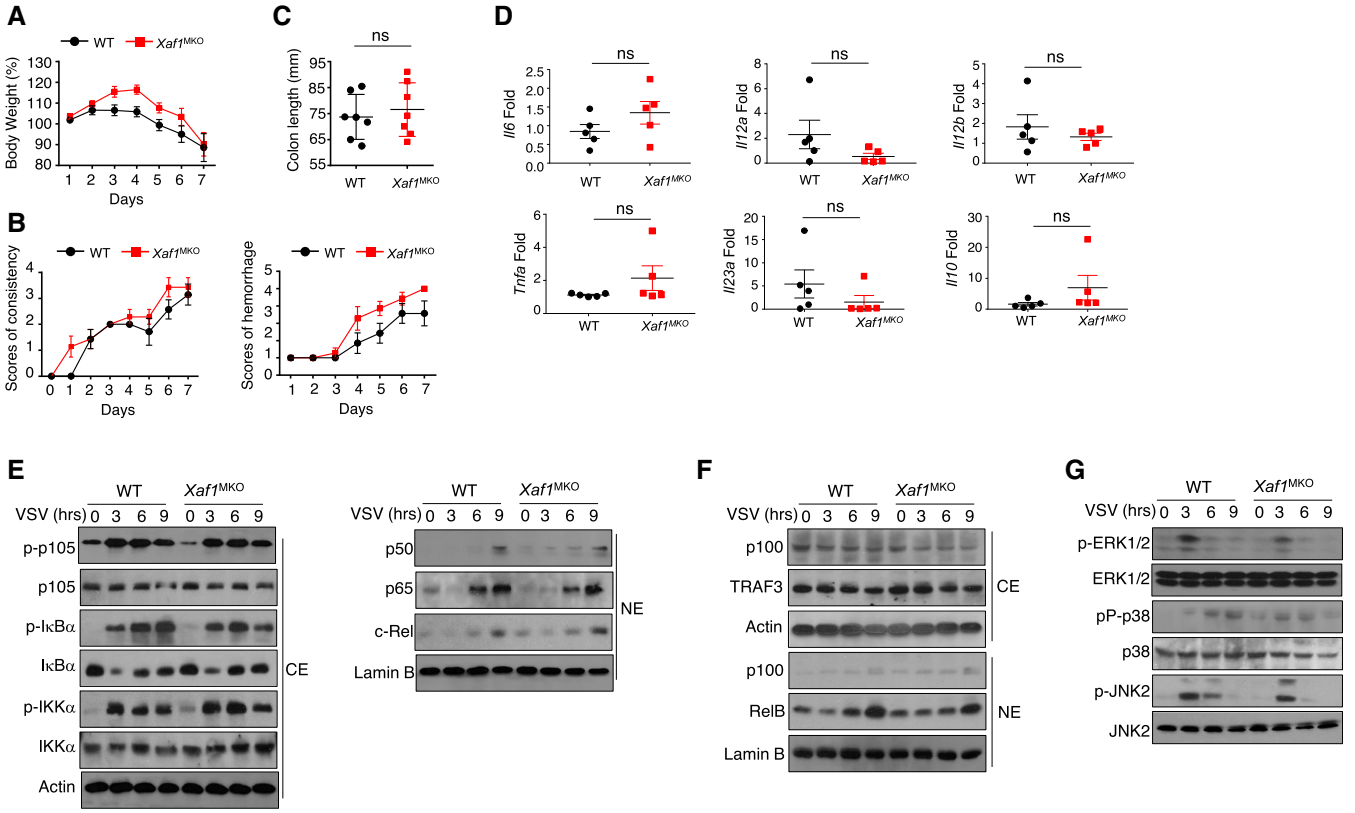

Figure EV2. No difference in the colitis model or activation of the MAPK and NF-κB pathways was observed between WT and XAF1^{MKO} mice.

A, B Body weight loss (A) and stool diarrhea and hematochezia scores (B) in WT and XAF1^{MKO} mice of the DSS-induced colitis model.

C, D Colon length (C) and proinflammatory cytokine production (D) of DSS-treated WT and XAF1^{MKO} mice on day 8.

E, F The indicated proteins in cytoplasmic (CE) and nuclear extracts (NE) of WT and XAF1-deficient BMDMs were detected by IB.

G The activation of MAPKs in total cell lysates was measured by IB.

Data information: The data are representative of at least three biologically independent experiments. Data from the qPCR assay are presented as the fold change relative to the *Actin* mRNA level. Data are represented as the means ± SDs. The significance of differences was determined by a *t*-test.
Source data are available online for this figure.

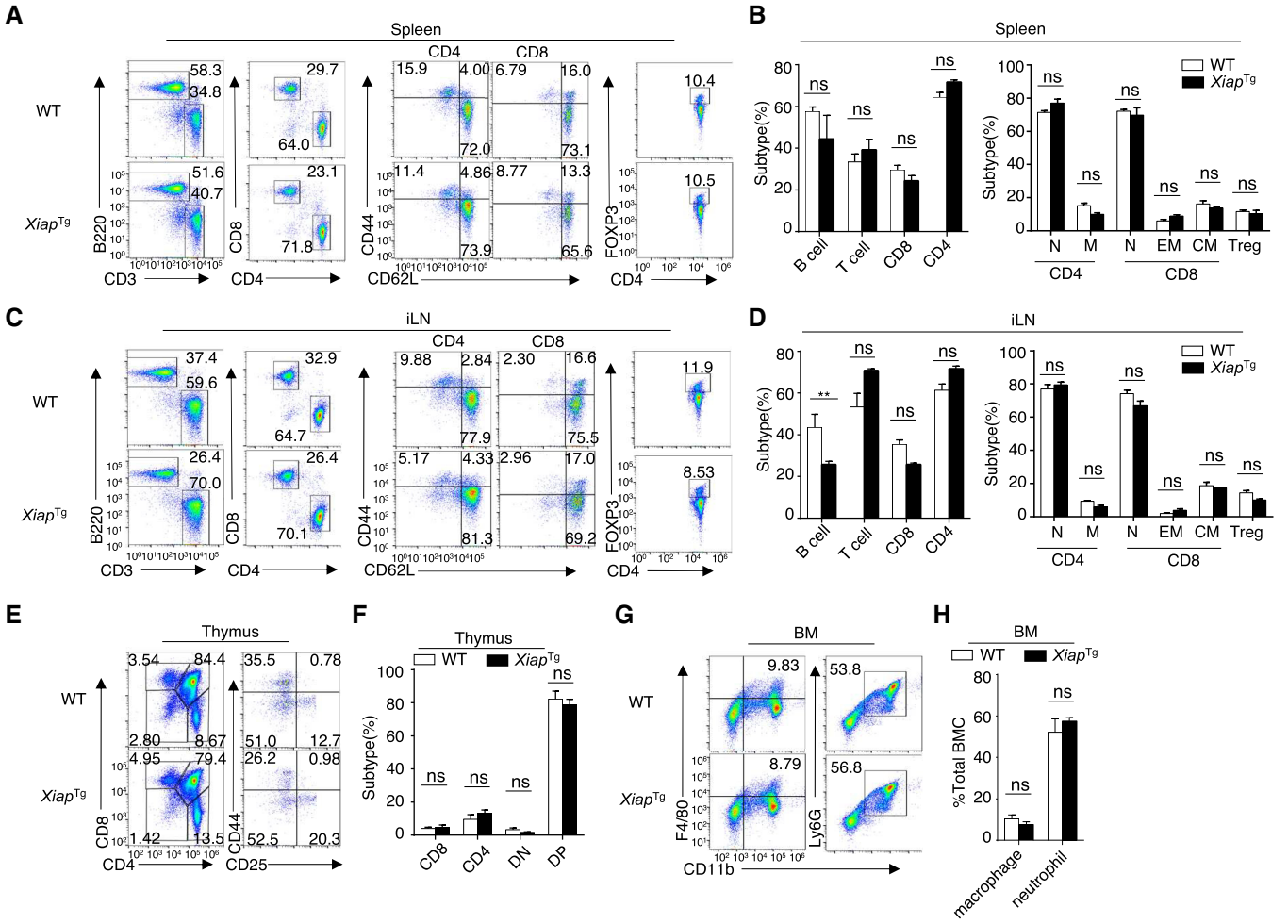

Figure EV3. XIAP is not required for the development of peripheral immune cells.

A–F Flow cytometry analysis of the absolute numbers of different immune cells in the spleen (A, B, upper), inguinal lymph nodes (C, D, middle), and thymus (E, F, lower) from WT and XAF1^{MKO} mice ($n = 3$).

G, H Flow cytometry analysis of macrophages (CD11b^{+}F4/80^{+}) and neutrophils (CD11b^{+}Ly6G^{+}) in bone marrow (BM) from 6- to 8-week-old WT and XAF1^{MKO} mice ($n = 3$).

Data information: The data are representative of at least three biologically independent experiments. Data are represented as the means ± SDs. The significance of differences was determined by *t*-tests. $^{**}P < 0.01$.

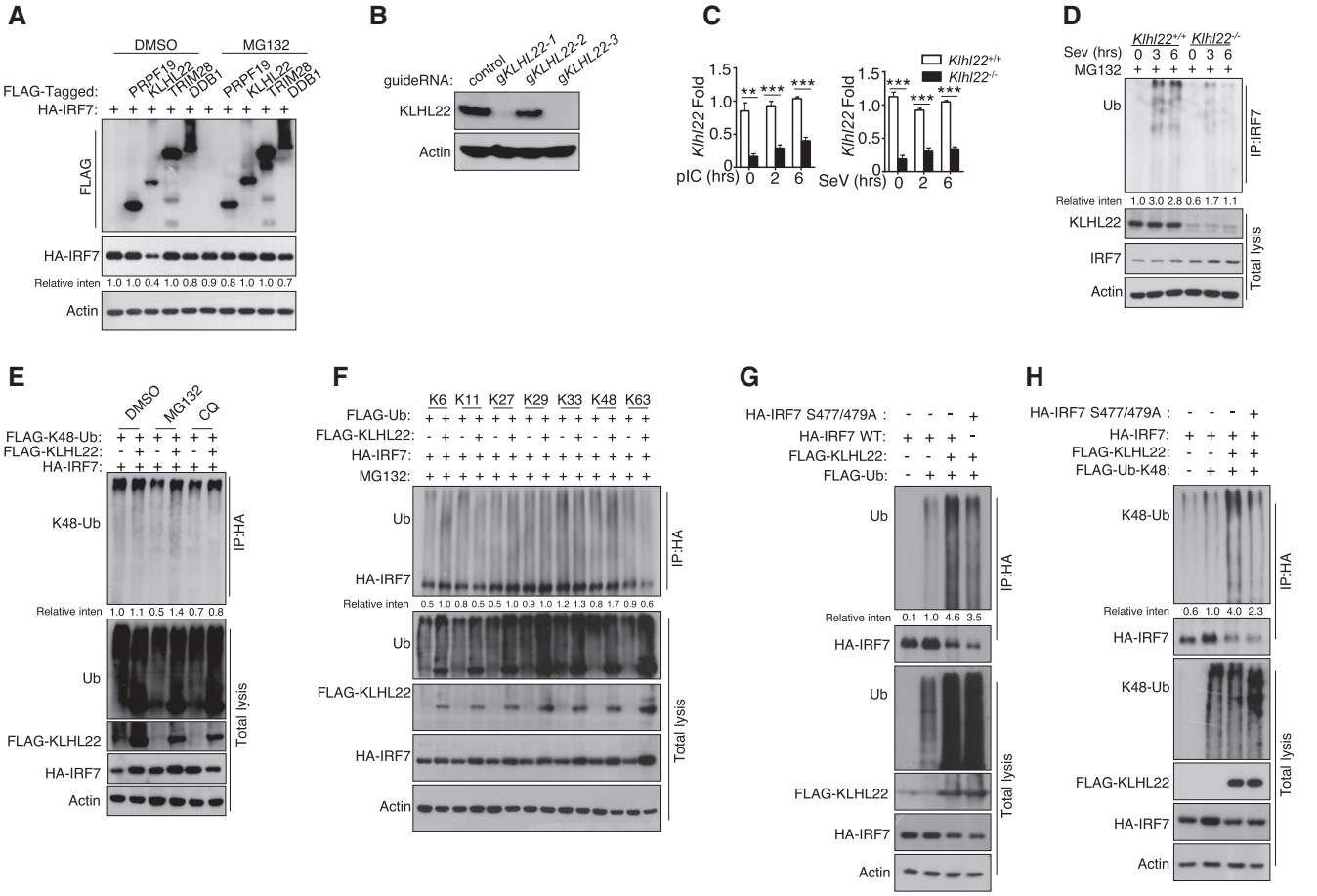

Figure EV4. KLHL22 mediates K48-linked ubiquitination of IRF7 and promotes its degradation.

A HEK293T cells were transfected with IRF7 and the indicated expression plasmids. After treatment with MG132, the indicated proteins were detected by IB.

B, C IB and qRT–PCR analysis showing specific ablation of KLHL22 in KLHL22-KO MEFs generated by CRISPR.

D After treatment with MG132, IRF7 was isolated by IP from whole-cell lysates (WLs) of KLHL22-KO MEFs and subjected to IB using anti-ubiquitin. Total cell lysates were also subjected to direct IB.

E HEK293T cells were transfected with IRF7 and FLAG-K48-ubiquitin in the presence (+) or absence (–) of KLHL22 expression plasmids. After pretreatment with MG132 or CQ, HA-tagged IRF7 was isolated by IP, and the ubiquitination level was then measured by IB.

F HEK293T cells were transfected with multiple ubiquitin mutants (mutations at K6, K11, K27, K29, K33, K48, and K63) and the indicated expression plasmids. HA-tagged IRF7 was isolated by IP, and the ubiquitination level was then measured by IB.

G, H HEK293T cells were transfected with HA-tagged IRF7 and the inactive mutant variants (S477 and 479A) whose phosphorylation sites at serine 477 and 479 were mutated from serine to alanine. HA-tagged IRF7 was isolated by IP, and the ubiquitination level was then measured by IB.

Data information: Data from the qPCR assay are presented as the fold change relative to the *Actin* mRNA level. Data are represented as the means ± SDs. The data are representative of at least three biologically independent experiments.
Please see Appendix Fig S7 for information regarding replicates, quantification, and statistical evaluation for biochemical data in this figure.
Source data are available online for this figure.

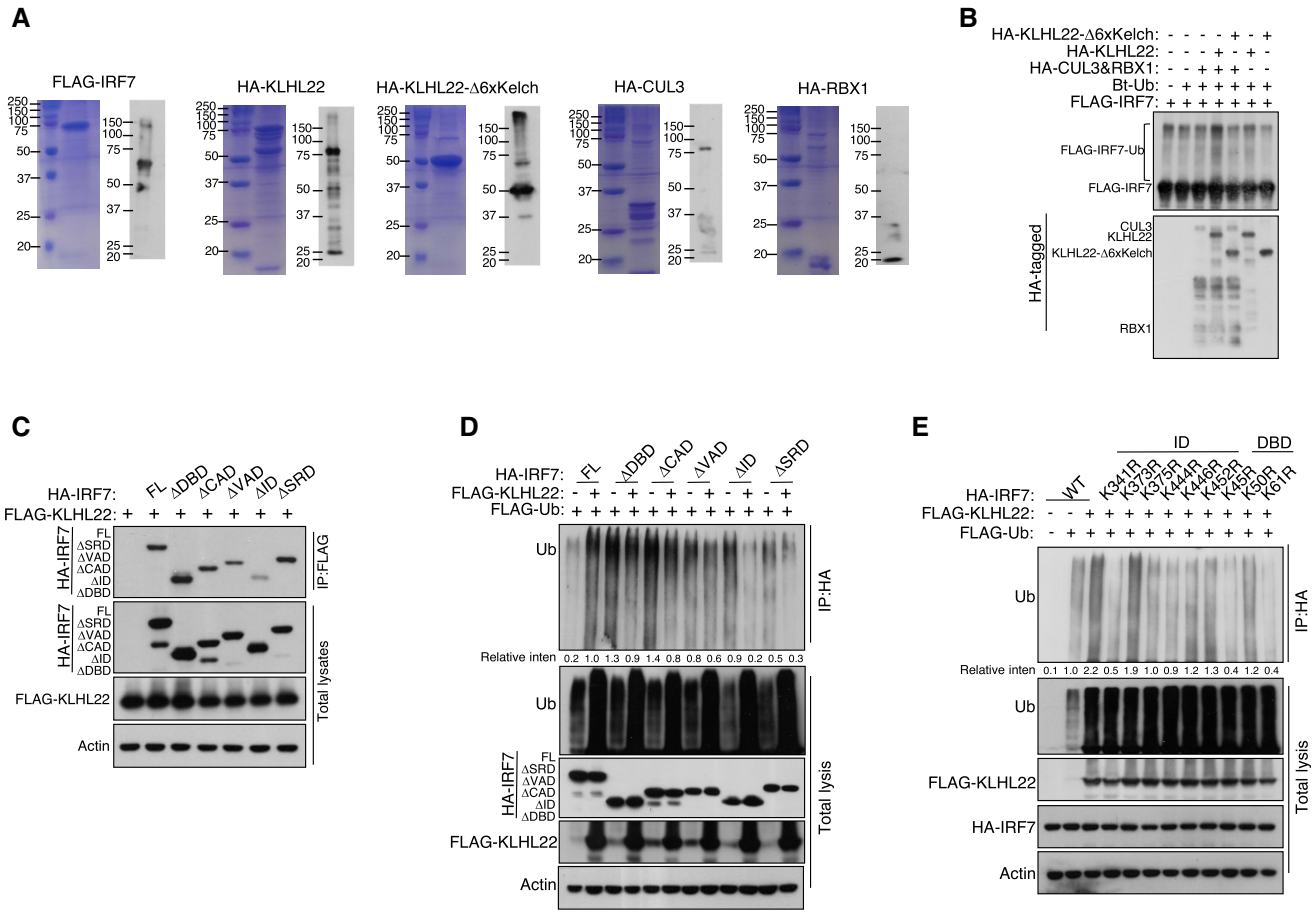

Figure EV5. KLHL22 interacts with IRF7 and promotes its ubiquitination.

A Purification of recombinant proteins was performed by Coomassie blue staining and IB.

B CUL3-KLHL22 E3 ligase catalyzed IRF7 ubiquitination in a cell-free system. Ubiquitin and recombinant FLAG-IRF7 were incubated with recombinant CUL3–RBX1 and KLHL22 or KLHL22-Δ6xKelch.

C The associations between KLHL22 and various truncations of IRF7 were detected through the indicated IP and IB analyses.

D HEK293T cells were transfected with KLHL22 and IRF7 variants. IB of FLAG was performed followed by IP with an anti-HA antibody.

E HEK293T cells were transfected with KLHL22, FLAG-ubiquitin, and various IRF7 point mutants. IB of FLAG was performed, followed by IP with an anti-HA antibody. The data are representative of at least three biologically independent experiments.

Data information: Please see Appendix Fig S8 for information regarding replicates, quantification, and statistical evaluation for biochemical data in this figure.
Source data are available online for this figure.